Materials & Design 227 (2023) 111803

Contents lists available at ScienceDirect

Materials & Design

journal homepage: www.elsevier.com/locate/matdes

Targeted Micro-Phase separation – A generic design concept to control the elasticity of extrudable hydrogels

Bruna R. Maciel [a,*], Ke Wang [a], Marc Müller [a], Claude Oelschlaeger [a], Norbert Willenbacher [a]

[a] Institute for Mechanical Process Engineering and Mechanics, Applied Mechanics Group. Karlsruhe Institute of Technology (KIT). Gotthard-Franz street 3, Build. 50.31, 76131 Karlsruhe, Germany

HIGHLIGHTS

- A new design concept that allows the mechanical strength of injectable gels to be adjusted based on micro-heterogeneities formation.
- Concept is valid for biocompatible polymeric as well as particulate extrudable hydrogels typically used in biomedical applications.
- Higher elasticity without increasing polymer/particle concentration or adding chemical crosslinker allows for improved filament extrusion at same printing conditions.

GRAPHICAL ABSTRACT

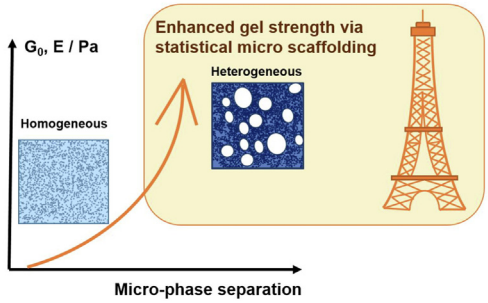

ARTICLE INFO

Article history:
Received 23 December 2022
Revised 24 February 2023
Accepted 27 February 2023
Available online 3 March 2023

Keywords:
Micro-heterogeneity
Micro-phase
Elasticity
Hydrogel
Extrusion

ABSTRACT

Hydrogels are ubiquitous in nature and technology. Controlling their mechanical properties and understanding their complex microstructure is critical e.g. for 3D bioprinting or tissue engineering applications. Here a generic design concept for tuning the elasticity of extrudable gels at given polymer or particle concentration is presented. Targeted micro-phase separation leading to micro-heterogeneities (1–100 μm) yields high gel strength allowing for extrusion of uniform filaments with high shape accuracy as long as the heterogeneity length scale is small compared to the extruded filament diameter (>500 μm). Micro-mechanical and structural heterogeneity was enhanced in alginate hydrogels by accelerating crosslinking kinetics, corresponding to gel elasticity variation of more than two orders of magnitude (17 Pa to 2300 Pa), enabling filament extrusion (1046 μm) with high shape fidelity. Introducing poly (vinylalcohol) into gelatin gels resulted in more heterogeneous materials with a 2-fold increase in elasticity (951 Pa to 1993 Pa) and thinner filaments (908 μm to 590 μm). Higher ionic strength in Laponite-based hydrogels induced nanoparticle aggregation, leading to higher elasticity (857 Pa to 2316 Pa) enabling smooth filament extrusion. Eliminating the often tacitly assumed hydrogel uniformity on the microscale provides additional degrees of freedom to achieve high gel strength without increasing polymer, particle or crosslinker concentration.

1. Introduction

Gels are ubiquitous in nature and technology. Hydrogels essentially consist of polymeric networks that retain expressive amount of water [1]. Extensive hydrogel research reports major advances

* Corresponding author.
E-mail address: bruna.maciel@kit.edu (B.R. Maciel).

https://doi.org/10.1016/j.matdes.2023.111803
0264-1275/

in cell encapsulation [2,3], contact lenses fabrication, drug delivery, wound healing, tissue engineering [4–6], biosensing technologies [7], agricultural applications [8,9], personal care products [10], food products [11], treatment of textile effluent [12], as well as dewatering and separation membranes [13,14].

Mechanical strength is an important design feature for all kinds of hydrogels. This property is directly related to texture perception in food gels [11,15], sensory and organoleptic properties of cosmetics [16], mechanical robustness of filtration membranes [14] and stability of adsorbent gels [17]. In addition, varying degrees of mechanical stiffness in biopolymer gels were found to influence the extra-cellular matrix synthesis of chondrocytes [18], and the differentiation of mesenchymal stem cells [19]. More specifically, mechanical strength can dictate injectability of hydrogels for therapeutic procedures and 3D bioprinting [20,21]. Extrudable hydrogels are a desired class of materials for 3D bioprinting applications, such as cardiac and skin tissue engineering, wound dressing as well as drug screening models [22]. Hydrogels consisting of biopolymers, i.e alginate [19] and gelatin [23], as well as nanoparticles, namely Laponite [24], are often employed as injectable materials. Injectability is characterized by the pressure required for flow as well as extrusion uniformity [25]. Therefore, the viscoelastic properties of both polymeric and particulate networks strongly dictate extrusion success.

The viscoelastic properties of polymeric gels strongly depend on the density of physical and/or chemical crosslinks, on polymer concentration, and hence the mesh size of the polymer network. For hydrogels these parameters are related to the swelling ratio which is controlled, e.g. by solvent quality, pH or ionic strength. Accordingly, various theoretical models have been derived to describe the gel elasticity, taking into account entropic as well as enthalpic contributions to the free energy. Most prominent, different types of polymer networks exhibit different scaling of the shear modulus $G_0 \sim c^{\alpha}$ with polymer concentration. All these models developed to describe the elasticity of (bio)polymer gels and networks have in common that they assume a uniform, homogenous sample composition on length scales larger than the individual molecules or filaments. Besides, commonly applied strategies for enhancing hydrogel elasticity involve increase in polymer/particle concentration, addition of reinforcement, such as particles or fibers, or chemical crosslinkers to polymer matrix as well as polymer matrix manipulation [26,27].

Here a new concept for tailoring the strength of typical extrudable polymeric and particulate hydrogels is presented, which abandons the assumption of uniformity. Targeted introduction of micro-heterogeneities can be used to tailor the mechanical strength of gels in a wide range which is decisive for the performance of such materials in injection, extrusion or 3D printing processes. This work was motivated by earlier investigations on commercial polymeric thickener solutions, which revealed that the thickening efficiency drastically increased for systems showing a heterogeneous structure on a mesoscopic length scale (1–10 μm) including predominately viscous and elastic regions. A certain shear modulus level was achieved at an almost ten times lower polymer concentration when compared with other thickeners with similar chemical composition but uniform structure on the mesoscopic scale [28]. Rubinstein proposes that nonlinear elasticity of polymer networks is generated by single polymer chain nonaffine deformations and Basu et. al reports on how such deformations in a polyacrylamide gel are caused by network crosslinking inhomogeneity (length scale $\sim$ 200 nm) [29,30]. Evidences of mechanical strength control through micro-structural heterogeneity are found by Bansil et al. [31] which, performing particle-tracking microrheology, found first indications that the elasticity of gastric mucus is related to its heterogeneity in a length scale 500 nm $-$ 4 μm.

Even in hard sphere suspensions the micro-phase separation into fluid regions of low particle concentration and small densely packed crystals at the entropy driven fluid-crystal phase transition results in a dramatic increase in viscosity and the formation of gel-like viscoelastic response [32]. Flocculated suspensions with their fractal particle network structure often exhibit high shear moduli even at low particle concentration [33]. Capillary suspensions (ternary fluid/fluid/solid systems) with their heterogeneous particle network typically exhibit shear moduli at least one order of magnitude higher than the corresponding binary suspensions [34]. In addition, Laponite nanoclay suspensions constitute thixotropic gels in the presence of electrolyte due to the formation of micro-meter sized nanoparticle aggregates (length scale < 5 μm) [35]. However, in Laponite phase diagrams, Laponite gels and glasses are addressed as uniform states and there is no indication in literature of phase separation for Laponite concentration > 1 wt% and salt concentration lower than 20 mM [36].

In this study, four different strategies for inducing micro-phase separation in extrudable hydrogels are presented, namely variation of crosslinking kinetics in a polysaccharide hydrogel, crosslinking of one polymer in a two-polymer mixture, variation of ionic strength in a nanosilicate hydrogel and formation of polysaccharide/nanosilicate composites. At a given polymer/nanoparticle and crosslink density, the hydrogels elastic modulus increases with increasing degree of micro-phase separation. An improved filament at constant extrusion pressure is observed as a direct effect of elasticity enhancement. The self-assembly of heterogeneous, micro-cellular structures results in a superior specific strength of the materials. In analogy to the well-known concepts in construction and engineering mechanics, we term this "statistical micro-scaffolding".

In this study, Multiple Particle Tracking (MPT) microrheology is employed to investigate microstructural changes and characterize micro-heterogeneity of the hydrogels in the hydrated state on a length scale 0.1–100 μm. Voronoi triangulation and image overlay techniques help direct visualization of spatial micro-heterogeneities formed inside the hydrogels, as demonstrated with the recently introduced Micro-Rheo-Mapping MRM tool [37]. This MPT technique is particularly suitable to visualize and characterize microscale heterogeneities in highly swollen gels. Unlike other microscopy techniques, MPT takes advantage of strong variations in local viscoelastic properties that often occur even if the local variation of the polymer or particle concentration is too small to generate enough contrast. Classical rotational rheometry as well as uniaxial compression tests were conducted to determine bulk elasticity. 3D printing is employed for injectability and extrusion quality evaluation. A correlation between micro-heterogeneities and their characteristics, such as size and degree of phase separation, and the macro elasticity of hydrogels is stablished, as well as the effects on the extrusion quality, demonstrating that targeted micro-phase separation is a generic design concept to control hydrogels elasticity and hence their injectability, extrudability or 3D printability.

2. Materials and methods

2.1. Sample preparation

Sodium alginate (alginic acid sodium salt from brown algae for biochemistry, M_w = 300–350 kg/mol), gelatin extra pure (gold, 180 Bloom), calcium chloride ($CaCl_2$) > 98% dehydrated and calcium sulfate ($CaSO_4$) > 98% dihydrate were purchased from Carl Roth (Karlsruhe, Germany). Poly(vinyl alcohol) (PVA, Mowiol ® 4–98, Mw $\sim$ 27000 g/mol) was purchased from Sigma- Aldrich Chemie

GmbH (Taufkirchen, Germany). Dulbecco's Modified Eagle's Medium (DMEM w: 4.5 g/L Glucose, w: L-Glutamine, w: Sodium pyruvate, w/o: Phenol red, w: 3.7 g/L $NaHCO_3$) was purchased from PAN Biotech (Aidenbach, Germany). D-Glucono-1.5-lacton (GDL) > 99% was purchased from Alfa Aesar (Thermo Fisher Scientific, Karlsruhe, Germany). Calcium carbonate ($CaCO_3$, Ulmer Weiss 15H) was purchased from Eduard Merkle GmbH (Blaubeuren-Altental, Germany). Laponite-XLG XR was purchased from BYK-Chemie GmBH (Wesel, Germany).

Salt and polymer solutions were prepared the following way: $CaCl_2$, $CaSO_4$, GDL solutions were prepared stirring the powder with ultrapure Milli-Q water at room temperature and approximately 100 rpm for ten minutes. Using the same procedure, alginate solutions were prepared (with longer stirring time of two hours) for systems I and II.a), but DMEM was used as solvent for system IV (see Table 1). DMEM is frequently employed as solvent in hydrogels used for cell culture as it provides nutrients and physiological conditions for the living cells (salt concentration: 0.2g/L $CaCl_2$, 0.4g/L KCl and 6.4g/L NaCl). Gelatin and PVA solutions were obtained using the same procedure as for alginate solutions, but stirring occurred using DMEM at 40 °C and ultrapure water at 90 °C, respectively. The $CaCO_3$ suspension was produced stirring the powder with ultrapure water.

Polymer hydrogels were prepared the following way: Alginate hydrogels were made ready by mixing alginate solution with the $CaCl_2$ solution, $CaCO_3$ suspension and GDL in order to solubilize $CaCO_3$ for ten minutes at 100 rpm (system I, see Table 1). The molar ratio $CaCO_3$:GDL was always kept 2:1. Two-polymer hydrogels were prepared by mixing PVA with the second polymer solution (gelatin or alginate followed by salt $CaSO_4$) for ten minutes at 100 rpm (system II, see Table 1). Hydrogels containing nanoparticle were produced the following way: Laponite nanoparticles were dispersed in ultrapure water with a planetary mixer (Speedmixer, Hauschild GmbH & Co KG, Hamm, Germany) for 10 min at 2500 rpm. Laponite hydrogels were prepared by mixing Laponite suspensions with salt solutions for 3 min at 2500 rpm using the planetary mixer (system III, see Table 1) and Laponite composites were prepared by mixing alginate solution with the Laponite suspension for 10 min at 2500 rpm (system IV, see Table 1). All samples in system III presented a pH value of 10, except for 3 wt% Laponite + 3 mM $Al_2(SO4)_3$ with pH = 7.6. All samples in system IV presented a pH value of 9.5.

Considering the well-known phenomenon of Laponite aging, all measurements were conducted 24 h after sample preparation for all systems investigated here. Table 1 shows the composition details and final weight concentrations of the different ingredients for the investigated systems.

2.2. Macrorheology: Rotational rheometry and uniaxial compression

A rotational rheometer (Rheoscope I, Thermo Fisher Scientific, Karlsruhe, Germany), equipped with a stainless-steel plate-plate measuring cell (diameter 20 mm, gap distance 2 mm) was used to perform small amplitude oscillatory shear experiments at 20 °C. Sandpaper was attached to the parallel plates in order to avoid slip. For all gels, frequency sweeps, covering the frequency range from 0.1 to 100 rad.s^{-1}, were performed at a stress amplitude sufficiently small to provide a linear material response. In oscillatory shear, a sinusoidal stress $\tau(t)$ is applied $\tau(t) = \tau_A . \sin \omega t$, where τ_A is the amplitude and ω the angular frequency. The linear response of the strain is given by $\gamma(t) = \gamma_A . \sin(\omega t + \delta)$, where δ is the phase shift angle. The shear stress $\tau(t)$ is proportional to the strain amplitude γ_A and can be represented as $\tau(t) = \gamma_A.(G\prime(\omega)(\sin(\omega t) + G\prime\prime(\omega)(\cos(\omega t))$. $G\prime(\omega)$ is defined as the storage modulus and $G\prime\prime(\omega)$ as the loss modulus. The storage and loss modulus are the real and imaginary parts of the complex modulus $G^*(\omega) = G'(\omega) + iG\prime\prime(\omega)$. The storage modulus represents the storage of elastic energy while the loss modulus indicates the viscous dissipation during strain cycle [33]. For polymer networks, the storage modulus G' is almost independent of frequency. Therefore, the bulk shear modulus G_0 is deduced from the value of G' at frequency ω = 1 rad.s^{-1}. The plateau modulus G_0 is a key structural parameter for entangled solutions and networks, it is related to the crosslinking density or mesh size of the entanglement network.

Uniaxial unconfined compression tests were performed at 20 °C using the commercial tensile testing machine Texture Analyzer TA. XTplus (Stable Micro System, UK) equipped with a 5 kg load cell. Tests were performed on cylindrically shaped gels of 5 mm height and 10 mm diameter. Samples were compressed with a plate (5 cm × 5 cm) at a compression speed of 0.1 mm/s. Young's modulus E was determined as the slope of the linear stress–strain curve in the strain region < 40%.

2.3. Microrheology: Multiple-particle tracking (MPT). A detailed scheme of the MPT setup used in this study is described in Kowalczyk et al. [28] It is based on an inverted fluorescence widefield microscope (Axio Observer D1, Carl Zeiss) equipped with a Fluar 100x objective (numerical aperture 1.3, 100x magnification, oil immersion lens, Carl Zeiss). Green fluorescent carboxyl-functionalized polystyrene microspheres of 0.2 μm diameter with density 1.06 g/cm^3 and refractive index 1.59 at 589 nm were used as tracer particles (Bangs Laboratories, USA).

The investigated samples including the tracer particles were placed between a microscope glass slide and a coverslip. The microscope was focused roughly halfway into the sample, i.e. at a distance of 20–40 μm away from the surface, to minimize wall effects. 2D images (field of view 127 × 127 μm, frame rate 50 frames/sec) of the fluorescent particles were recorded using a sCMOS camera Zyla X (Andor Technology). Movies of the fluctuating microspheres were analyzed using a custom MPT routine incorporated into the software Image Processing System (Visiometrics iPS). Particle tracking and calculation of mean square displacement (MSD), as well as the statistical analysis of the trajectories was done using a self-written Matlab® program based on the widely used Crocker and Grier tracking algorithm [28]. Tra-

Table 1
Detailed composition of hydrogel systems I-IV.

System	I	II				III	IV
		a		b			
Polymer	1.2% alginate	1.2% alginate	PVA (0–2.8%)	8% gelatin	PVA (0–4%)	-	alginate (0–2%)
Solvent	H_2O	H_2O	H_2O	DMEM	H_2O	–	DMEM
Salt	0.16% ($CaCl_2$ +$CaCO_3$) + GDL	0.16% $CaSO_4$		–		4 mM NaCl 15 mM (NaCl + KCl) 4 mM $CaCl_2$ 3 mM $Al_2(SO_4)_3$	–
Nanoparticle	–	–		–		3% Laponite	5% Laponite

cer particles were added prior to gelation, to ensure a homogeneous distribution of the tracer particles within the sample. The local viscoelastic modulus $G^*(\omega)$ around a sphere as a function of the frequency ω can be determined from Eq. (1) [38]:

$$G*(\omega) = \frac{k_b T}{\pi a i\omega \left\langle \tilde{\Delta r}^2 (i\omega) \right\rangle} = G'(\omega) + iG''(\omega) \quad (1)$$

with a being the tracer particle radius, k_B the Boltzmann constant, T the temperature and $\langle \tilde{\Delta r}^2(i\omega) \rangle$ the Mean Square Displacement (MSD) of the tracer particles.

Tracers trapped in an elastic network exhibit a time-independent MSD directly related to the apparent local shear modulus (Eq.2) of this region:

$$G_{0,MPT} = \frac{2k_B T}{3\pi a \Delta r^2} \quad (2)$$

Tracers freely diffusing in a viscous environment exhibit a linearly increasing MSD and the apparent viscosity η_{MPT} of the surrounding fluid is determined using Eq. (3) obtained from the Stokes-Einstein relation, and the relation $\langle \Delta r^2(\tau) \rangle = 4D\tau$, where D is the diffusion coefficient related to the MSD $\langle \Delta r^2(\tau) \rangle$ as a function of the lag time τ [39]:

$$\eta_{MPT} = \frac{k_B T}{6\pi a D} \quad (3)$$

In this study we investigate heterogeneous systems. MPT allows for the evaluation of heterogeneity in terms of the non-Gaussian parameter α *(alfa)*. Details on the non-Gaussian parameter, which describes the deviation of the MSD values from a Gaussian distribution, are given in the Supplementary Information (Table S1).

2.4. Hydrogel extrusion. A pressure-controlled Voxel 8 Developer's Kit 3D printer (Voxel 8 Inc., Harvard, USA), 3CC cartridges (Nordson EFD, Feldkirchen, Germany) and straight needles of stainless steel, (150 µm outlet diameter, VIEWEG, Germany), were used to extrude the hydrogels in log pile pattern (self-written G-Code). The print head velocity was kept at 600 mm/min for all samples and the extrusion pressure was system dependent, varying from 0.03 MPa to 0.4 MPa. The extruded constructs were imaged using a Digital Microscope VHX-950F (Keyence, Neu-Isenburg, Germany) and image analysis was performed with the software Image Processing System (Visiometrics iPS).

2.5. Statistical analysis. Data are expressed as mean ± SD. Comparisons between two experimental groups were performed using two-tailed t tests with $N \geq 3$ for all groups. Differences were statistically significant for $P < 0.05$.

3. Results and discussion

This investigation employs four different hydrogel systems, each one presenting a different mechanism of inducing phase separation (Table 2) on the length scale 1 – 100 µm. MPT microrheology technique is used to characterize these heterogeneities and their effect on bulk elasticity is discussed.

3.1. System I – Varying crosslinking kinetics in alginate/calcium salt hydrogels

Physically crosslinked hydrogels are formed when calcium ions interact with alginate guluronate blocks, originating the so-called egg-box model structure [40]. The ionic crosslinking kinetics in alginate gels is determined by the calcium salt solubility in water and therefore by the diffusion rate of the Ca^{2+} ions in the system.

Two Ca^{2+}-salts with very different solubility were used, $CaCl_2$ (solubility of 745 mg/mL at 20 °C), which delivers instantaneous crosslinking and $CaCO_3$ (solubility of 0.02 mg/mL at 20 °C) [41], with a crosslinking time > 10 min (47). Alginate (1.2 wt%) as well as the total salt (0.16 wt%) concentrations are kept constant, while the $CaCl_2$:$CaCO_3$ weight ratio is varied.

The heterogeneous microstructure shows up in a broad variation in absolute values and time dependence of the individual MSDs for all gels in this concentration series (as shown in Fig. S1). The ensemble of MSDs is arbitrarily classified in two main populations, as shown exemplarily in Fig. 1A for $CaCl_2$:$CaCO_3$ ratio 1:1. MSDs with slope < 0.5 (black population in Fig. 1A) correspond to tracer particles trapped in predominantly elastic regions. Predominantly viscous regions are characterized by tracer particles diffusing freely in the surrounding fluid, corresponding to MSDs with slope > 0.5 (green population in Fig. 1A).

Voronoi triangulation has been used to visualize the heterogeneity of the samples [28], where the black and green areas represent elastic and viscous regions, respectively (see Fig. 1b for $CaCl_2$:$CaCO_3$ ratio 1:1). Size of the viscous inclusions was estimated by means of Feret's statistical diameter using the public domain processing software ImageJ [42]. Viscous inclusions of size typically 10–20 µm and characteristic viscous area fraction of 10–40% are found (Fig. 1B).

Increasing the amount of $CaCl_2$ leads to a more pronounced phase separation. This is indicated by the decrease of apparent local viscosity in the viscous regions (green areas in Fig. 1b) from 115 mPas (corresponding to the viscosity of ~ 1 wt% alginate) to 1mPas (corresponding to the viscosity of water), and on the other side by the increase in the apparent local shear modulus $G_{0,MPT}$ in the elastic regions (black areas in Fig. 1B) from ~ 1 to 11 Pa (Fig. 1C). In an alginate hydrogel formed by adding only $CaCO_3$, the slow crosslinking process forms weakly crosslinked regions that coexist with uncrosslinked polymer solution. By partially substituting $CaCO_3$ for $CaCl_2$, the elastic regions become stronger crosslinked as more polymer takes part in this process. The polymer concentration decreases in the uncrosslinked inclusions, hence the viscosity also decreases. This clearly shows that the degree of phase separation and heterogeneity increases with higher fraction of fast crosslinker.

$CaCl_2$ high solubility and therefore high diffusion rate of calcium ions forms dense crosslinked zones that coexist with weak bonding sites or even uncrosslinked polymer as well as salt solution pools [43]. Because of the low solubility of $CaCO_3$, GDL is responsible for the slow dissolution of Ca^{2+} in the system. As the further diffusion rate of ions after the initial binding is also responsible for the degree of heterogeneity [44], a slower crosslinking

Table 2
Composition and micro-heterogeneity control mechanisms of the systems investigated.

System	I	IIa	IIb	III	IV
Material	Alginate + Ca^{2+} salts	Alginate + PVA	Gelatin + PVA	Laponite + salt	Laponite + alginate
Micro-phase separation mechanism	Variation of crosslinking kinetics by varying salt solubility	by adding second polymer	Demixing of micro-phases triggered via thermal crosslinking of one polymer	Nanoparticle cluster formation via variation of ionic strength	Nanoparticle/ polymer cluster formation via addition of polymer

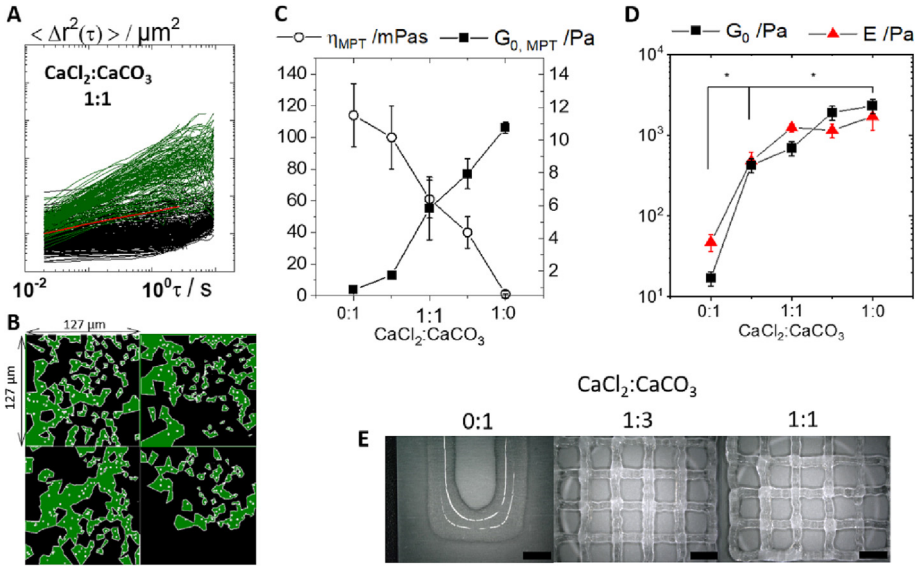

Fig. 1. Micro-heterogeneities and rheological characterization of System I. (**A**) Mean square displacement as a function of lag time τ for 1.2 wt% alginate with $CaCl_2$:$CaCO_3$ ratio 1:1. Green and black indicating viscous and elastic MSDs, respectively, and red ensemble average of MSDs. (**B**) Corresponding Voronoi plot as obtained from MPT measurements with tracer particles of diameter 0.2 μm. Four videos were analyzed and one representative MSD diagram is presented. (**C**) Apparent local viscosity η_{MPT} and apparent local elasticity $G_{0,MPT}$ as obtained by MPT measurements and (**D**) bulk shear modulus G_0 and Young's modulus E as obtained by shear rheometry and compression tests, respectively, as a function of $CaCl_2$:$CaCO_3$ ratio in 1.2 wt% alginate hydrogel (* indicates $P < 0.05$). (**E**) Extruded alginate hydrogels with $CaCl_2$:$CaCO_3$ ratio 0:1, 1:3 and 1:1. Scale bar = 3 mm. (For interpretation of the references to colour in this figure legend, the reader is referred to the web version of this article.)

process leads to weaker micro phase separation, delivering more homogeneous hydrogels [40,45].

The more pronounced micro-phase separation leads to a strong increase of two orders of magnitude in the bulk shear modulus G_0 from 17 to 2300 Pa and in the Young's modulus E from 48 to 1700 Pa (Fig. 1D). This stunning increment in the bulk elasticity at constant polymer and salt concentration is a consequence of the more pronounced micro-phase separation when the crosslinking process is accelerated due to the addition of a highly water-soluble salt. The bulk elastic modulus values found are much higher than the apparent local elasticity $G_{0,MPT}$. This might be due to densely crosslinked areas which are inaccessible to the tracer particles and therefore do not contribute to $G_{0,MPT}$ [46].

To our knowledge, microscopic dynamics and structure in alginate hydrogels have only been characterized in terms of dynamic light scattering (DLS) [43], revealing the presence of different relaxation modes and these dynamics were associated to the formation of a hierarchy of crosslinks with different lifetimes indicating a complex structure without, however, providing any spatial information about micro-heterogeneity. This study presents, for the first time, spatial characterization of viscous inclusions in hydrated alginate gels as well as local viscoelastic properties of the micro-phases.

The increase in gel elasticity with a higher fraction of the fast crosslinker ($CaCl_2$) shows improved extrusion results already at $CaCl_2$:$CaCO_3$ ratios 1:3 and 1:1 (Fig. 1.E). Gel with only $CaCO_3$ salt does not have enough cohesive strength for extrusion, thus the filament spreads and does not retain shape. The higher elastic gels due to increased micro-heterogeneity, on the other side, were successfully extruded in continuous and uniform filaments of width 1046 ± 170 μm at 0.17 MPa. These results clearly demonstrate that the heterogeneous structure and the degree of phase separation are decisive parameters for controlling the bulk elasticity and extrudability of alginate hydrogels.

3.2. System II – Crosslinking of one polymer in a two-polymer mixture

Turning to polymer composites, system II comprises mixtures of alginate/PVA and gelatin/PVA where only alginate and gelatin are crosslinked and PVA remains as solution in the hydrogel.

3.2.1. System II.a) – Variation of alginate crosslinking kinetics by the addition of PVA

As already discussed in the previous section, the addition of Ca^{2+} ions to alginate generates a hydrogel with certain degree of micro-heterogeneity. Adding PVA to a 1.2 wt% alginate solution prior to the addition of 0.16 wt% $CaSO_4$ (solubility of 2.41 mg/mL at 20 °C) [41], however, leads to significant modifications of the microstructure (Fig. 2A-B). Both viscous and elastic phases are present in all systems, but with a distinct disparity in tracer mobility between these regions for the sample without PVA.

When increasing the amount of PVA to 2.8 wt% and keeping the alginate and $CaSO_4$ concentrations constant, the viscosity η_{MPT} within the viscous regions increases from 138 mPas (corresponding to the viscosity of ~ 1 wt% alginate) to 307 mPas (mixed solution of alginate and PVA). Viscous inclusions typically 10 μm in size are found in all samples (Fig. 2C-D). In presence of PVA, the hydrogel evolves into a more homogeneous material as fewer viscous inclusions are formed and the average percentage of viscous area is reduced from 12 ± 1% to 3 ± 1%.

The microstructural changes observed in system II.a) can be explained by the interaction of alginate and PVA via hydrogen bonding of hydroxyl groups before addition of $CaSO_4$. Studies with XRD (x-ray diffraction) have shown that, as the quantity of alginate in a PVA/alginate blend nanofibers is increased, the intensity of the diffraction peak of PVA becomes lower and broader [47,48]. The reduction of the crystallinity of the electrospun PVA/alginate nanofibers can probably be attributed to the hydrogen-bonding interaction between alginate and PVA macromolecules. Besides, FTIR (Fourier-transform infrared spectroscopy) results have shown that, with the addition of alginate, the intensity of absorption peaks of PVA decrease, and some peaks disappear, suggesting an interaction between PVA and alginate [47,48]. It was also observed that the

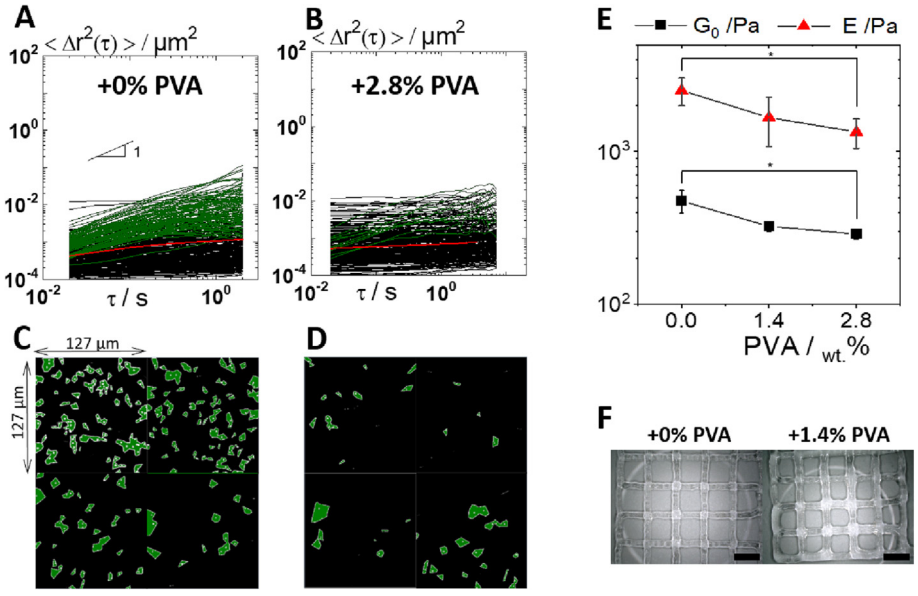

Fig. 2. Micro-heterogeneities and rheological characterization of System II.a). (**A**)-(**B**) Mean square displacement as a function of lag time τ for 1.2 wt% alginate and 1.2 wt% alginate + 2.8 wt% PVA. Green indicating viscous MSD, black elastic MSD and red ensemble average of MSDs. (**C**)-(**D**) Corresponding Voronoi plots as obtained from MPT measurements with tracer particles of diameter 0.2 µm. Viscous area fraction decreases in the alginate hydrogel as more PVA is present. For each concentration, four videos were analyzed and one representative MSD diagram is presented. (**E**) Bulk shear modulus G_0 as obtained by shear rheometry and Young's modulus E as obtained by compression tests as a function of PVA concentration in 1.2 wt% alginate + 0.16 wt% $CaSO_4$ hydrogel (* indicates $P < 0.05$). (**F**) Extruded alginate hydrogels with 0% and 1.4% PVA. Scale bar = 3 mm. (For interpretation of the references to colour in this figure legend, the reader is referred to the web version of this article.)

bands of hydroxyl stretching become much broader with adding alginate, which supports the idea that hydrogen bonding could be formed between alginate and PVA hydroxyl groups. Moreover, the fact that PVA molecular chain contains highly polar functional groups (hydroxyl) facilitates intermolecular interaction in the form of hydrogen bonding between PVA and alginate, resulting in a denser system [49].

On account of this, alginate crosslinking with Ca^{2+} ions is delayed and a more homogeneous hydrogel with lower degree of micro-phase separation is formed when PVA is introduced. As discussed previously, a slower crosslinking kinetics produces more homogeneous alginate hydrogels.

As a result of a lower micro-phase separation degree, a decrease in the macro-elasticity is observed (Fig. 2E). Both G_0 and E drop almost by a factor of 2 in presence of PVA. This is consistent with what was already observed for pure alginate gels, again a more heterogeneous microstructure leads to higher bulk elasticity at constant polymer concentration. The concentration of the polymer that actively participates in the crosslinking process and contributes to the elasticity, i.e. alginate, is kept constant while only PVA concentration is increased. An aqueous 2.8 wt% PVA solution, however, presents a viscosity lower than 4mPas, which clearly excludes any PVA entanglement contribution to the hydrogel elasticity. The change in micro-heterogeneity is the only source for the observed change in the gel's bulk elasticity.

The elasticity decrease in gels with PVA directly affects extrusion quality (Fig. 2.F). With the addition of 1.4% PVA to alginate gel, filament width increased from 676 ± 90 µm to 857 ± 171 µm when extruded at 0.17 MPa.

3.2.2. System II.b) demixing of gelatin/PVA micro-phases via thermal crosslinking of gelatin matrix

PVA is now incorporated into gelatin, which forms a physically crosslinked hydrogel via thermal gelation. Gelatin concentration is kept constant (8 wt%) while PVA solution concentration is increased from 0 to 4 wt%. Overlay plots created from 500 subsequent images taken from MPT video sequences (Fig. 3A-B) clearly reveal that a heterogeneous micro-structure results from the addition of PVA to gelatin [50].

A uniform particle distribution occurs in pure gelatin sample (Fig. 3A), while inclusions depleted of tracer particles are found in the samples with PVA (Fig. 3B). The size of these inclusions increases from 7.5 ± 3 µm at 2 wt% PVA content (Figure S2) to 15 ± 10 µm at 4 wt% PVA (Fig. 3B). At the same time, the area fraction of these inclusions in the hydrogel increased from 12% to 28%. All tracers are embedded in an elastic gel-like environment provided by the gelatin gel (Fig. 3C).

In order to characterize the void spaces, tracer particles were directly injected into the inclusions with a syringe (Fig. 3D). As shown exemplarily in Fig. 3E for sample 8 wt% gelatin + 4 wt% PVA, the tracer particles diffuse freely, indicating that these inclusions are presumably formed of aqueous PVA solution that demixed from the gelatin gel during the thermal crosslinking process. Samples with 2 wt% and 4 wt% PVA presented local apparent viscosity η_{MPT} in these pore shaped inclusions of 23mPas and 35mPas, respectively, corresponding to the viscosity of approximately 6 wt% and 7 wt% PVA.

This higher PVA content in the pores is a result of micro-phases demixing. Liquid-liquid as well as solid–liquid separation depend strongly on the concentration of the components and on the environmental stimuli, such as temperature or pH [51,52]. Crosslinking of one polymer in a mixture can induce micro-phase separation, as only one component is sensitive to the environmental stimuli or crosslinking reaction and the whole mixture becomes unstable. This method can be employed for producing controlled microstructured materials based on the kinetics of demixing [52].

In our study, gelatin and PVA (as well as tracer particles) were well mixed in the aqueous solution at 40 °C. By lowering the temperature, gelatin begins to thermally crosslink and the demixing process of gelatin network and PVA solution is triggered. By the time room temperature is reached (20 °C) further phase separation is ceased. At this point, the gelatin elastic network is stabilized along with the tracer particles, which were arrested in the elastic

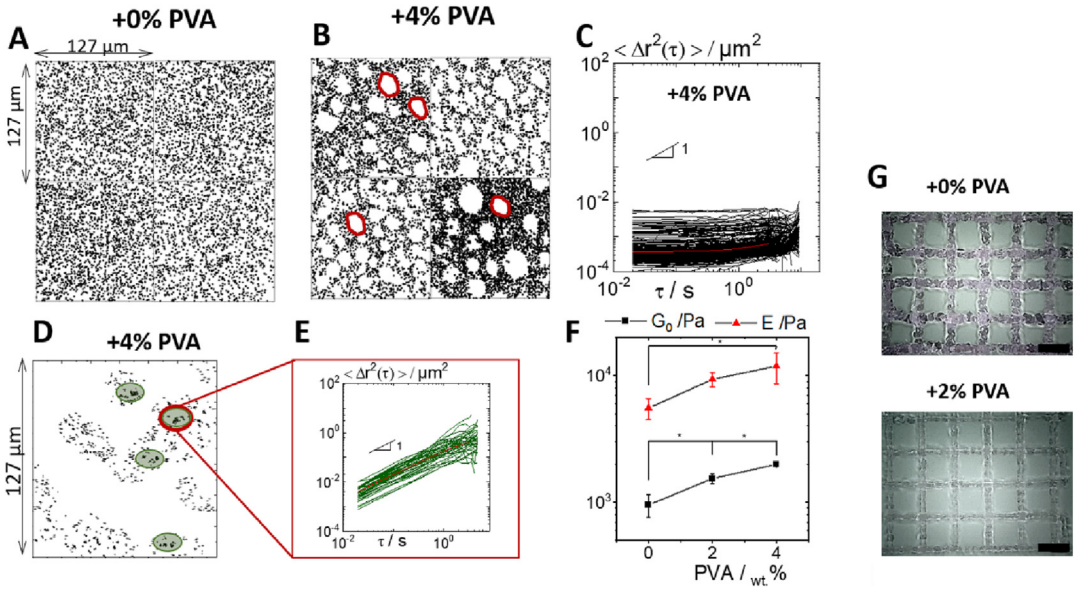

Fig. 3. Micro-heterogeneities and rheological characterization of System II.b). **(A)-(B)** Overlay plots for 8 wt% gelatin and 8 wt% gelatin + 4%$_{wt.}$PVA (four videos were analyzed for each concentration), some viscous inclusions are indicated in red, (**C**) representative MSDs of elastic trajectories as a function of lag time for 8 wt% gelatin + 4 wt% PVA, (**D**) overlay plot for tracer particles directly injected in viscous inclusions (green area), (**E**) representative MSDs of viscous trajectories for sample with 4 wt% PVA, as obtained by MPT measurements and (**F**) bulk shear modulus G_0 as obtained by shear rheometry and Young's modulus E as obtained by compression tests as a function of PVA concentration in 8 wt% gelatin hydrogel (* indicates $P < 0.05$). (**G**) Extruded gelatin hydrogels with 0% and 2% PVA. Scale bar = 3 mm. (For interpretation of the references to colour in this figure legend, the reader is referred to the web version of this article.)

phase during demixing, and PVA is found dispersed in discrete pore shaped viscous inclusions.

The micro-heterogeneities formed due to the addition of PVA to the system lead to an increase in the bulk elasticity of a factor of 2 for both G_0 and E (Fig. 3F)), even though the amount of polymer actively participating in the crosslinking process and therefore network formation, i.e. gelatin, is kept constant at 8 wt%. A 4 wt% aqueous PVA solution presents a viscosity ≈5 mPas, clearly excluding entanglement effects on the hydrogel overall elasticity. The micro-phases separation resulted in the formation of elastic regions with higher gelatin crosslinking density than in the pure gelatin gel and of viscous inclusions consisting of PVA with a higher viscosity in comparison to the mixture before demixing. This micro-phase demixing phenomenon is responsible for the increase in the overall hydrogel bulk elasticity.

Improved extruded filaments are obtained for the hydrogel with 2% PVA (590 ± 76 µm line width) in comparison to pure gelatin (908 ± 118 µm line width) at a constant extrusion pressure of 0.4 MPa (Fig. 3.G). The extrusion of thinner filaments, i.e. less spreading at the same pressure value is directly related to the higher elasticity at constant gelatin concentration.

3.3. System III – Varying ionic strength in Laponite hydrogels

Clay suspensions exhibit complex phase behavior depending on clay concentration, pH and ionic strength. For Laponite suspensions this has been extensively discussed e.g. in Ruzicka & Zaccarelli [36]. At pH < 11, Laponite platelets are negatively charged on their faces, but positively charged at the edges. In the absence of salt, an extended electrical double layer is formed around the particles in suspension and repulsive forces dominate. Addition of electrolyte to Laponite suspensions induces a contraction of the electrical double layer and attractive forces become relevant [53,54], leading to modifications in the microstructure.

For system III investigated here, Laponite suspensions ionic strength $I = 0.5\sum_{i=1}^{n} c_i z_i^2$, where c_i is ion concentration and z_i is the ion charge, was varied by the addition of salts with increasing concentration or cation valence. Tracer particles were homogeneously distributed in a salt free 3 wt% Laponite suspension, as shown in Fig. 4A. By adding 4 mM monovalent salt NaCl to 3 wt % Laponite suspension, almost no changes occur (data not shown). By increasing the concentration of monovalent salt from 4 to 15 mM however, large white areas where no tracer particles are present appear (Fig. 4B). Similar changes in the microstructure occur when divalent and trivalent cation salts, $CaCl_2$ and $Al_2(SO_4)_3$ respectively, are incorporated into 3 wt% Laponite suspension (Fig. 4C-D).

Densely packed areas inaccessible for the 200 nm tracer particles are formed at ionic strength ≥ 15 mM and/or when multivalent ions are added. This is due to short-range attraction among particles resulting from van der Waals interactions and different charge densities on the rims and faces of Laponite platelets [53,55]. The length scale of the inaccessible areas was found to be 20–100 µm and the average inaccessible area fraction in the hydrogel increased from 17 ± 5% (15 mM NaCl + KCl) to 37 ± 22% (3 mM $Al_2(SO_4)_3$) by increasing the salt cation valence. Such heterogeneous microstructures in Laponite suspensions have been suspected earlier based on dynamic light scattering and active micro rheology experiments [53]. Here, the size and shape of microstructure were visualized for the first time enabled by overlay plots of image series taken from MPT video sequences [50].

The tracer particles embedded in 3% Laponite gels sense only elastic microenvironment, as indicated by time independent MSDs exemplarily shown in Fig. 4E for 3 wt% Laponite + 4 mM $CaCl_2$. Similar results were obtained for all other systems investigated in this series (Fig. S3).

The increase in the ionic strength to values $I > 10$ mM accompanied by an enhanced micro-phases separation leads to a drastic growth in the bulk elasticity of the hydrogel at constant nanoclay concentration (Fig. 4F). For 3 $_{wt}$% Laponite with no salt, E increase from 860 Pa to 2315 Pa with the addition of 3 mM of trivalent salt. Changes in the macroelasticity of Laponite hydrogels when increasing ionic strength were reported in the literature and associated to aggregate formation based on DLS and small-angle X-ray

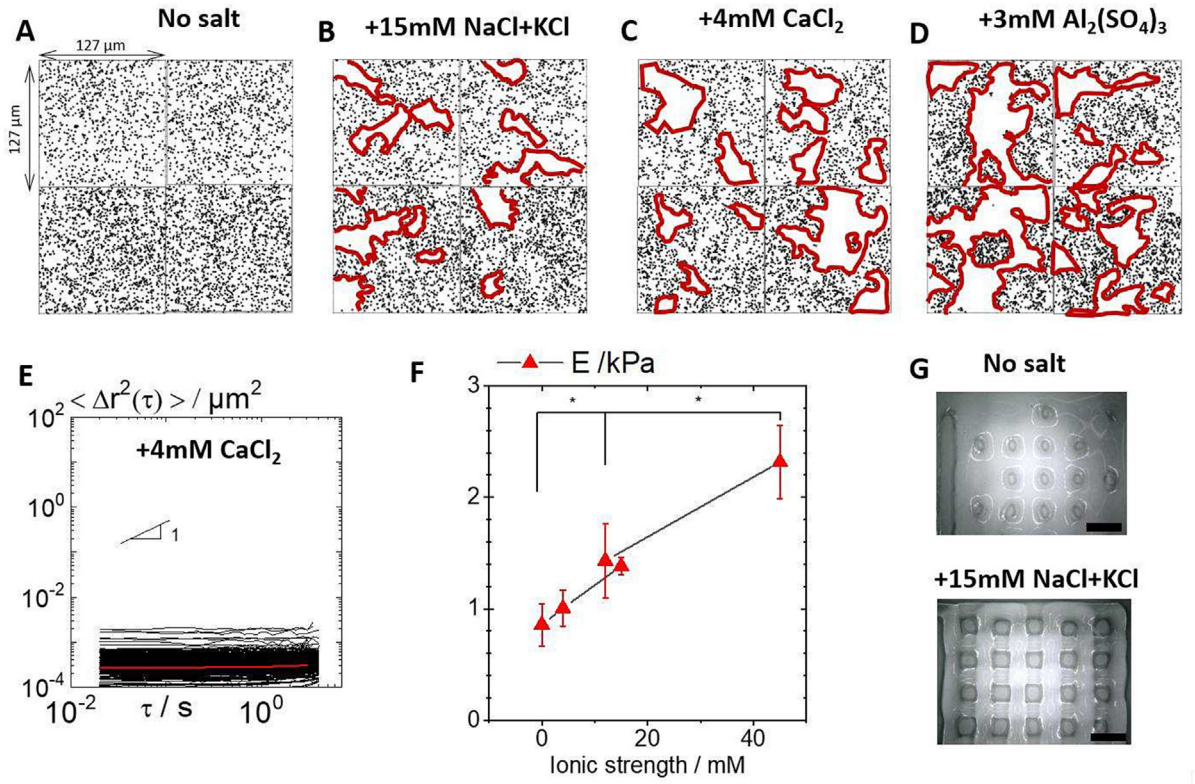

Fig. 4. Micro-heterogeneities and mechanical characterization of System III. **(A)-(D)** Overlay plots for pure 3 wt% Laponite XLG hydrogel and 3 wt% Laponite XLG hydrogel in the presence of salt with increasing ionic strength, clusters are indicated in red and (**E**) representative MSDs of elastic trajectories for 3 wt% Laponite + 4 mM $CaCl_2$, as obtained by MPT measurements. For each formulation, four videos were analyzed and one representative MSD diagram is presented. (**F**) Young's modulus E as obtained by compression tests and ionic strength values for pure 3 wt% Laponite hydrogel and 3 wt% Laponite hydrogel in the presence of salt with increasing ionic strength (* indicates $P < 0.05$). All samples in system III presented a pH value of 10, except for 3 wt% Laponite + 3 mM $Al_2(SO4)_3$ with pH = 7.6. (**G**) Extruded laponite hydrogels without salt and with 15 mM NaCl + KCl. Scale bar = 3 mm. (For interpretation of the references to colour in this figure legend, the reader is referred to the web version of this article.)

scattering (SAXS) experiments [56,57]. In our investigation, it was shown for the first time that a micro-phase separation on a length scale 10–100 µm is related to the strong increase in bulk elasticity upon increasing ionic strength.

Pure Laponite hydrogel did not form filaments when extruded, as the gel was not strong enough to retain shape (Fig. 4.G). The addition of 0.15 mM of monovalent salt increased gel elasticity and allowed uniform extrusion of 1324 ± 137 µm wide filaments at 0.03 MPa without increasing nanoparticle concentration.

3.4. System IV – Cluster formation in Laponite/alginate composites

Microstructural alterations in Laponite based hydrogels may occur not only upon variation of ionic strength but also by adding polymers. Micro-heterogeneities were formed and tracer particles were no longer found homogeneously distributed when 1 wt% alginate in DMEM was added to a 5 wt% Laponite hydrogel (Fig. 5A,B). Densely packed regions typically 20–40 µm in diameter and depleted of tracer particles are found presumably consisting of mixed Laponite alginate aggregates.

By further increasing alginate concentration up to 2 wt% (Fig. 5C) and keeping Laponite concentration constant, the frequency of clusters decreases and the hydrogel becomes more homogeneous again. When Laponite particles interact with polymer chains dissolved in solvent containing electroctrolyte, such as DMEM, compact clusters of nanoclay and polymer are formed [57,58]. However, when increasing the amount of alginate but keeping electrolyte concentration constant, hydrogen bonding as well as electrostatic interactions between Laponite particles and alginate chains hinder nanoparticle cluster formation, thus leading to a more homogeneous hydrogel [59]. Similar to system III, MSD of all tracers in system IV are time independent (data not shown).

The formation of micro-heterogeneities upon addition of 1 wt% alginate is accompanied by a sharp rise in the bulk elasticity, followed by gradual decline in G_0 and E as the fraction of dense aggregates decreases when the alginate concentration is further increased (Fig. 5D). It should be noted that alginate is not cross-linked in the system, so it does not contribute to the elasticity by creating an elastic polymeric network but by inducing aggregate formation and micro-phase separation with Laponite in the presence of electrolyte. The non-monotonic variation of bulk elasticity can be directly related to the degree of micro-heterogeneity in this sample series. This further confirms the hypothesis that targeted micro-phase separation is a powerful tool to control bulk elasticity of composite gels. It is worth noting that in Systems I and IV, G_0 and E show very similar values, while in System II, $E > G_0$. For ideal uniform, isotropic bodies, $E = 3G_0$. However, the systems investigated here are not ideal uniform and isotropic, so this relation may vary depending on the structural features of the micro-heterogeneities. Besides, these differences in G_0 and E might be explained by the diverse deformation processes polymer chains undergo depending on the hydrogel loading mode. The different microstructural deformations in a hydrogel under shear and under compression might result in different macro mechanical properties. Knapp describes distinct G_0 and E values for collagen hydrogels due to distinct reactions of collagen fibrils upon deformation by shear and by compression [60].

The increase in elasticity in system IV via addition of 1 wt% alginate solution to Laponite gels did not improve filament extrusion (Fig. 5.E). The amount and size of the nanoclay/polymer clusters

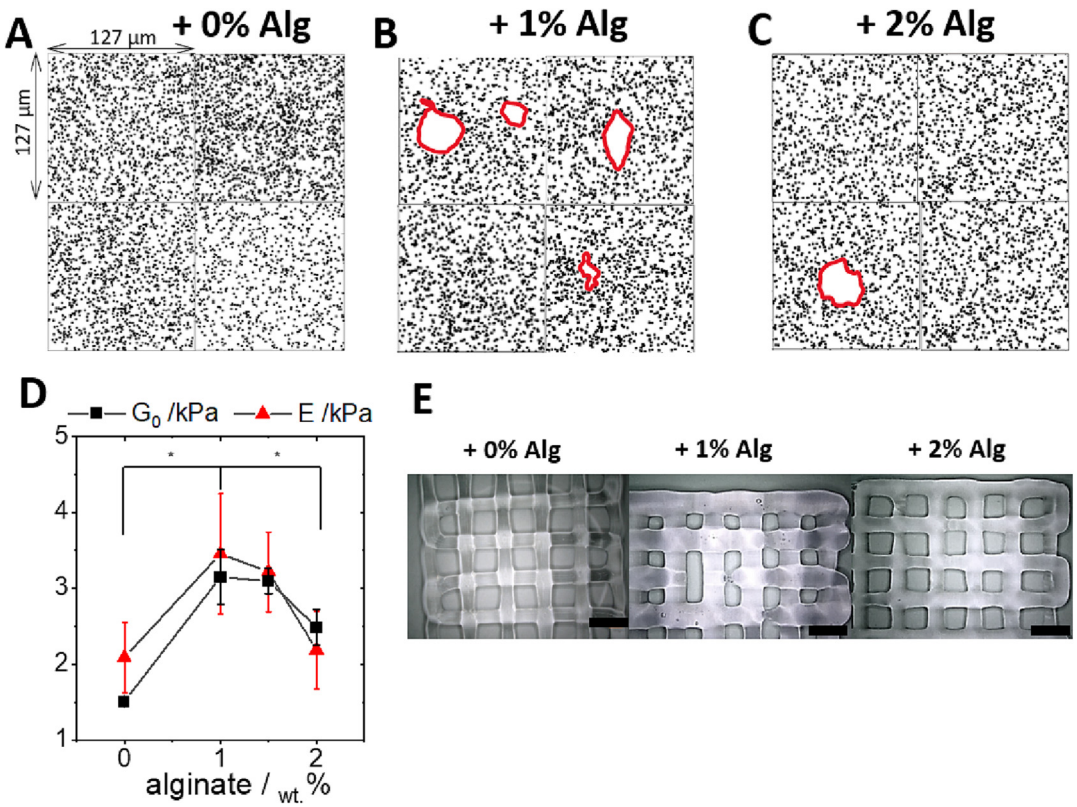

Fig. 5. Micro-heterogeneities and mechanical characterization of System IV**. (A-C**): Overlay plots for pure 5 wt% Laponite XLG hydrogel and 5 wt% Laponite XLG hydrogel with alginate, clusters are indicated in red (four videos were analyzed for each concentration) and (**D**) bulk shear modulus G_0 and Young's modulus E as obtained by shear rheometry and compression tests, respectively, as a function of alginate concentration in 5 wt% Laponite in DMEM hydrogel (* indicates $P < 0.05$). All samples in system IV presented a pH value of 9.5. (**E**) Extruded Laponite hydrogels with 0%, 1% and 2% alginate. Scale bar = 3 mm. (For interpretation of the references to colour in this figure legend, the reader is referred to the web version of this article.)

might impair filament uniformity and continuous extrusion. This effect was not studied here, and further investigations will be performed to characterize impact of micro-heterogeneity characteristics on 3D printing performance in more detail. The further decrease in elasticity with addition of 2 wt% alginate to Laponite produced continuous filaments of 1253 ± 186 µm width at 0.4 MPa in comparison to 789 ± 40 µm for pure Laponite at 0.07 MPa.

Even though no improvement in the extrusion quality was observed with the addition of alginate to Laponite, the hydrogel remained injectable with continuous filament extrusion. Nanoclay/polymer composites are of interest for biomedical application where the presence of both polymeric and particulate materials influence cell behavior.

3.5. Statistical micro-scaffolding design concept

It is demonstrated that targeted micro-phase separation is a generic design concept to control the elasticity of extrudable hydrogels. Several strategies are presented for introducing micro-heterogeneities in a hydrogel matrix via micro-phase separation which resulted in an increase in gel elasticity at a given polymer or particle concentration. The increase in gel strength happens regardless of the heterogeneity state of matter. These micro-heterogeneities can appear as viscous inclusions in the gel matrix, as demonstrated in System I, with inclusions formed of uncrosslinked alginate and salt solutions, and in System II, where inclusions of PVA solution phase separated from the gelatin gel during thermal crosslinking. Strategies where solid micro-heterogeneities were formed are presented in System III, with nanoparticle aggregates and in System IV with aggregates constituted of Laponite and alginate.

This novel design concept, does not require polymer chain modification, reinforcement or chemical crosslinker addition to increase hydrogel strength. The concept was applied to a broad variety of different hydrogel systems, showing that this generic approach can be widely employed for designing polymer and particulate hydrogels, even a transfer to organogels seems to be straightforward. The specific strategy for inducing micro-heterogeneities depends on the system composition, as demonstrated in this study. Different material compositions will have particular requirements for triggering micro-phase separation in order to reach a micro-heterogeneity intensity relevant for strength enhancement. Polymer or particle concentration might also dictate the characteristic features of achievable micro-heterogeneities. Thorough understanding of how the hydrogel components interact with each other is the basis for a targeted and efficient micro-phase separation leading to an increase in elasticity. If these specific boundary conditions are known, a transfer of the design concept to other systems not investigated here should be straight forward.

Regarding the thermodynamics of micro-phase separation, the process is determined by the interfacial free-energy, which is mainly influenced by the interfacial area [61]. Micro-phase separation has been reported to occur in hydrogels when thermo-sensitive polymer segments become hydrophobic at temperatures higher than the critic temperature $T > T_c$ and separate from hydrophilic segments, which have more affinity with water molecules. These thermo-sensitive segments which became hydrophobic form local micellization, shrinking while separating from the

hydrophilic phase. This local shrinkage and overall deswelling results in increase in the bulk hydrogel elasticity. The hydrogel obeys the rubber elasticity rule, as the thermoresponsive segments are hydrophilic when $T < T_C$ and the swelling is more pronounced. When $T > T_C$, the local shrinkage due to micro-phase separation causes the increase of the elastic modulus. As reported for a PNIPAm/PDMA (poly(N-isopropylacrylamide)/poly(N,N-dimethylacrylamide)) hydrogel, a further increase in temperature enhances the degree of micro-phase separation and the elasticity is increased significantly due to shrinkage of the thermoresponsive PNIPAm segments [61]. In this case, however, the length scale (<100 nm) and the underlying physical mechanism of phase separation are different from the systems investigated here.

For the extrudable hydrogels studied here, micro-heterogeneity formation and the corresponding elasticity increase improved dispensing or extrusion quality at constant printing conditions. The increase in elasticity enabled extrusion of uniform filaments with high shape fidelity in systems I and III, while thinner lines could be printed in system II. An elasticity enhancement via conventional ways, such as increasing the crosslink density or adding reinforcement fillers usually leads to an increase in the extrusion pressure necessary for printing uniform filaments. Finally, the length scale of the introduced heterogeneities was kept small (1–100 μm) compared to the extrude filament diameter (>500 μm). This is mandatory to ensure high printing quality in terms of filament uniformity and shape fidelity.

The statistical micro-scaffolding design concept is relevant to hydrogel design applications such as 3D bioprinting, tissue engineering, wound dressing or drug screening, where extrudability is desired or required but high compressive or shear stresses could be detrimental. Furthermore, this design concept may have implications for various applications where both mechanical strength and heterogeneity of the hydrogel are important, e.g. in texture, sensory and organoleptic properties perception, mechanical robustness of filtration and adsorbent gels, or in the differentiation of stem cells embedded in hydrogels with varying degrees of stiffness.

4. Conclusion

A new generic design rule is presented, that allows the mechanical strength of polymeric and particulate extrudable gels to be adjusted based on the formation of heterogeneities on the length scale 1–100 μm. This concept abandons the assumption of uniform sample composition tacitly assumed in essentially all theories referring to the viscoelastic behavior of gels, and offers additional degrees of freedom for enhancing mechanical gel strength without increasing polymer / particle concentration or average crosslink density. In this study, different polymeric and particulate model systems were used to demonstrate the feasibility of the strategy and the impact on extrudability.

Micro-mechanical and structural heterogeneity was enhanced in alginate hydrogels by accelerating crosslinking kinetics, generating higher elastic materials (17 Pa to 2300 Pa) with substantially improved filament extrudability and shape fidelity (1046 ± 170 μm wide filaments). Adding PVA prevented alginate crosslinking and produced softer (475 Pa to 289 Pa), more homogeneous hydrogels, with larger extruded filament width. Introducing PVA into gelatin gels resulted in more heterogeneous materials with higher elasticity (951 Pa to 1993 Pa) and therefore thinner extruded lines (908 ± 118 μm to 590 ± 76 μm) due to micro-phase separation. Higher ionic strength in Laponite-based hydrogels induced nanoparticle aggregation, producing materials of higher elasticity (857 Pa to 2316 Pa) and superior extrusion quality (1324 ± 137 μm wide filaments). Further addition of alginate prevented cluster formation due to nanoparticle-polysaccharide interactions, resulting in more homogeneous, softer materials with larger filament spreading (789 ± 40 μm to 1253 ± 186 μm).

These findings provide deeper insight into complex hydrogel micro-structures in the hydrated state and expand our capabilities to control bulk mechanical gel properties. With the design concept developed in this study, increase in gel elasticity and improvement in filament extrusion are possible maintaining constant extrusion conditions. The length scale of the heterogeneity, however, was kept much smaller (1–100 μm) than the extrude filament diameter (>500 μm) in order to ensure uniform, interruption-free extrusion. Further investigations should be carried on the impact of micro-heterogeneity size, type and volume fraction on the shape fidelity and uniformity of extruded hydrogel filaments and how this depends on specific system properties.

In addition, this design model may have implications in several applications in which hydrogel mechanical strength as well as heterogeneity are relevant, namely food and cosmetic gels, as well as hydrogels used for tissue engineering and bioprinting.

Triggered self-assembly into a "statistical microcellular" structure is a generic design strategy that can be used to tune the elasticity of gels over a wide range. Following the well-known design scheme from engineering mechanics, it is referred to here as the statistical micro-scaffolding concept.

Data availability Statement.

Data will be made available on request.

CRediT authorship contribution statement

Bruna R. Maciel: Conceptualization, Data curation, Formal analysis, Investigation, Methodology, Supervision, Validation, Visualization, Writing – original draft, Writing – review & editing. **Ke Wang:** Formal analysis, Investigation, Visualization. **Marc Müller:** Formal analysis, Investigation, Visualization. **Claude Oelschlaeger:** Conceptualization, Data curation, Methodology, Project administration, Supervision, Writing – original draft, Writing – review & editing. **Norbert Willenbacher:** Conceptualization, Methodology, Funding acquisition, Project administration, Resources, Supervision, Writing – original draft, Writing – review & editing.

Data availability

Data will be made available on request.

Declaration of Competing Interest

The authors declare that they have no known competing financial interests or personal relationships that could have appeared to influence the work reported in this paper.

Acknowledgements

The authors declare that the project was funded by the basic budget of our institute provided by the state ministry of science, research, and art of Baden-Württemberg.

Appendix A. Supplementary data

Supplementary data to this article can be found online at https://doi.org/10.1016/j.matdes.2023.111803.

References

[1] E.M. Ahmed, Hydrogel: Preparation, characterization, and applications: A review, Journal of advanced research 6 (2015) 105–121, https://doi.org/10.1016/j.jare.2013.07.006.

[2] G.D. Nicodemus, S.J. Bryant, Cell encapsulation in biodegradable hydrogels for tissue engineering applications, Tissue engineering, Part B, Reviews 14 (2008) 149–165, https://doi.org/10.1089/ten.teb.2007.0332.

[3] M. Villiou, J.I. Paez, A. Del Campo, Photodegradable Hydrogels for Cell Encapsulation and Tissue Adhesion, ACS applied materials & interfaces 12 (2020) 37862–37872, https://doi.org/10.1021/acsami.0c08568.

[4] E. Caló, V.V. Khutoryanskiy, Biomedical applications of hydrogels: A review of patents and commercial products, European Polymer Journal 65 (2015) 252–267, https://doi.org/10.1016/j.eurpolymj.2014.11.024.

[5] G. Chen, W. Tang, X. Wang, X. Zhao, C. Chen, Z. Zhu, Applications of Hydrogels with Special Physical Properties in Biomedicine, Polymers 11 (2019), https://doi.org/10.3390/polym11091420.

[6] S. Correa, A.K. Grosskopf, H. Lopez Hernandez, D. Chan, A.C. Yu, L.M. Stapleton, E.A. Appel, Translational Applications of Hydrogels, Chemical reviews 121 (2021) 11385–11457, https://doi.org/10.1021/acs.chemrev.0c01177.

[7] A. Herrmann, R. Haag, U. Schedler, Hydrogels and Their Role in Biosensing Applications, Advanced healthcare materials 10 (2021) e2100062.

[8] M. Klein, E. Poverenov, Natural biopolymer-based hydrogels for use in food and agriculture, Journal of the science of food and agriculture 100 (2020) 2337–2347, https://doi.org/10.1002/jsfa.10274.

[9] T.J. Gutiérrez, Polymers for Agri-Food Applications, Springer International Publishing, Cham, 2019.

[10] A. Bashari, A. Rouhani Shirvan, M. Shakeri, Cellulose-based hydrogels for personal care products, Polym Adv Technol 29 (2018) 2853–2867, https://doi.org/10.1002/pat.4290.

[11] H. Khalesi, W. Lu, K. Nishinari, Y. Fang, New insights into food hydrogels with reinforced mechanical properties: A review on innovative strategies, Advances in colloid and interface science 285 (2020), https://doi.org/10.1016/j.cis.2020.102278 102278.

[12] S. Bhattacharya, R. Shunmugam, Polymer based gels and their applications in remediation of dyes from textile effluents, Journal of Macromolecular Science, Part A 57 (2020) 906–926, https://doi.org/10.1080/10601325.2020.1782229.

[13] S.-L. Loo, L. Vásquez, A. Athanassiou, D. Fragouli, Polymeric Hydrogels—A Promising Platform in Enhancing Water Security for a Sustainable Future, Adv Materials Inter 8 (2021) 2100580, https://doi.org/10.1002/admi.202100580.

[14] M.K. Yazdi, V. Vatanpour, A. Taghizadeh, M. Taghizadeh, M.R. Ganjali, M.T. Munir, S. Habibzadeh, M.R. Saeb, M. Ghaedi, Hydrogel membranes: A review, Materials science & engineering, C, Materials for biological applications 114 (2020), https://doi.org/10.1016/j.msec.2020.111023 111023.

[15] M.A. Cerqueira, L.H. Fasolin, C.S.F. Picone, L.M. Pastrana, R.L. Cunha, A.A. Vicente, Structural and mechanical properties of organogels: Role of oil and gelator molecular structure, Food research international (Ottawa, Ont.) 96 (2017) 161–170, https://doi.org/10.1016/j.foodres.2017.03.021.

[16] R.M. Martinez, C. Rosado, M.V.R. Velasco, S.C.S. Lannes, A.R. Baby, Main features and applications of organogels in cosmetics, International journal of cosmetic science 41 (2019) 109–117, https://doi.org/10.1111/ics.12519.

[17] Y. Seida, H. Tokuyama, Hydrogel Adsorbents for the Removal of Hazardous Pollutants-Requirements and Available Functions as Adsorbent, Gels 8 (2022), https://doi.org/10.3390/gels8040220.

[18] J. Jang, Y.-J. Seol, H.J. Kim, J. Kundu, S.W. Kim, D.-W. Cho, Effects of alginate hydrogel cross-linking density on mechanical and biological behaviors for tissue engineering, Journal of the mechanical behavior of biomedical materials 37 (2014) 69–77, https://doi.org/10.1016/j.jmbbm.2014.05.004.

[19] F.E. Freeman, D.J. Kelly, Tuning Alginate Bioink Stiffness and Composition for Controlled Growth Factor Delivery and to Spatially Direct MSC Fate within Bioprinted Tissues, Scientific reports 7 (2017) 17042, https://doi.org/10.1038/s41598-017-17286-1.

[20] T. Birman, D. Seliktar, Injectability of Biosynthetic Hydrogels: Consideration for Minimally Invasive Surgical Procedures and 3D Bioprinting, Adv. Funct. Mater. 31 (2021) 2100628, https://doi.org/10.1002/adfm.202100628.

[21] M. Guvendiren, H.D. Lu, J.A. Burdick, Shear-thinning hydrogels for biomedical applications, Soft Matter 8 (2012) 260–272, https://doi.org/10.1039/c1sm06513k.

[22] A. Raza, M. Mumtaz, U. Hayat, N. Hussain, M.A. Ghauri, M. Bilal, H.M. Iqbal, Recent advancements in extrudable gel-based bioinks for biomedical settings, Journal of Drug Delivery Science and Technology 75 (2022), https://doi.org/10.1016/j.jddst.2022.103697 103697.

[23] Y. Wang, R.K. Kankala, K. Zhu, S.-B. Wang, Y.S. Zhang, A.-Z. Chen, Coaxial Extrusion of Tubular Tissue Constructs Using a Gelatin/GelMA Blend Bioink, ACS biomaterials science & engineering 5 (2019) 5514–5524, https://doi.org/10.1021/acsbiomaterials.9b00926.

[24] F.-F. Cai, S. Heid, A.R. Boccaccini, Potential of Laponite® incorporated oxidized alginate-gelatin (ADA-GEL) composite hydrogels for extrusion-based 3D printing, Journal of biomedical materials research, Part B, Applied biomaterials 109 (2021) 1090–1104, https://doi.org/10.1002/jbm.b.34771.

[25] F. Cilurzo, F. Selmin, P. Minghetti, M. Adami, E. Bertoni, S. Lauria, L. Montanari, Injectability Evaluation: An Open Issue, AAPS PharmSciTech 12 (2011) 604–609, https://doi.org/10.1208/s12249-011-9625-y.

[26] D. Ji, J. Kim, Recent Strategies for Strengthening and Stiffening Tough Hydrogels, Adv NanoBio Res 1 (2021) 2100026, https://doi.org/10.1002/anbr.202100026.

[27] C. Xu, G. Dai, Y. Hong, Recent advances in high-strength and elastic hydrogels for 3D printing in biomedical applications, Acta biomaterialia 95 (2019) 50–59, https://doi.org/10.1016/j.actbio.2019.05.032.

[28] A. Kowalczyk, C. Oelschlaeger, N. Willenbacher, Visualization of micro-scale inhomogeneities in acrylic thickener solutions: A multiple particle tracking study, Polymer 58 (2015) 170–179, https://doi.org/10.1016/j.polymer.2014.12.041.

[29] M. Rubinstein, S. Panyukov, Nonaffine Deformation and Elasticity of Polymer Networks, Macromolecules 30 (1997) 8036–8044, https://doi.org/10.1021/ma970364k.

[30] A. Basu, Q. Wen, X. Mao, T.C. Lubensky, P.A. Janmey, A.G. Yodh, Nonaffine Displacements in Flexible Polymer Networks, Macromolecules 44 (2011) 1671–1679, https://doi.org/10.1021/ma1026803.

[31] R. Bansil, J.P. Celli, J.M. Hardcastle, B.S. Turner, The Influence of Mucus Microstructure and Rheology in Helicobacter pylori Infection, Frontiers in immunology 4 (2013) 310, https://doi.org/10.3389/fimmu.2013.00310.

[32] J. Mewis, N.J. Wagner, Colloidal Suspension Rheology, University Press, Cambridge, United Kingdom, 2012.

[33] R.G. Larson, The structure and rheology of complex fluids, Oxford University Press, New York, 1999.

[34] E. Koos, N. Willenbacher, Capillary forces in suspension rheology, Science (New York, N.Y.) 331 (2011) 897–900. https://doi.org/10.1126/science.1199243.

[35] F. Pignon, A. Magnin, J.-M. Piau, B. Cabane, P. Lindner, O. Diat, Yield stress thixotropic clay suspension: Investigations of structure by light, neutron, and x-ray scattering, Phys. Rev. E 56 (1997) 3281–3289, https://doi.org/10.1103/PhysRevE.56.3281.

[36] B. Ruzicka, E. Zaccarelli, A fresh look at the Laponite phase diagram, Soft Matter 7 (2011) 1268, https://doi.org/10.1039/c0sm00590h.

[37] C. Oelschlaeger, J. Marten, F. Péridont, N. Willenbacher, Imaging of the microstructure of Carbopol dispersions and correlation with their macroelasticity: A micro- and macrorheological study, Journal of Rheology 66 (2022) 749–760, https://doi.org/10.1122/8.0000452.

[38] T.G. Mason, Estimating the viscoelastic moduli of complex fluids using the generalized Stokes-Einstein equation, Rheologica Acta 39 (2000) 371–378, https://doi.org/10.1007/s003970000094.

[39] W. Mason, Optical measurements of frequency-dependent linear viscoelastic moduli of complex fluids, Physical review letters 74 (1995) 1250–1253, https://doi.org/10.1103/PhysRevLett.74.1250.

[40] C.K. Kuo, P.X. Ma, Ionically crosslinked alginate hydrogels as scaffolds for tissue engineering: Part 1, Structure, gelation rate and mechanical properties, Biomaterials 22 (2001) 511–521, https://doi.org/10.1016/S0142-9612(00)00201-5.

[41] A.M. Comey, A Dictionary of Chemical Solubilities: Inorganic, McMillan & Co., New York, 1921.

[42] W.H. Walton, Feret's Statistical Diameter as a Measure of Particle Size, Nature 162 (1948) 329–330, https://doi.org/10.1038/162329b0.

[43] D. Larobina, L. Cipelletti, Hierarchical cross-linking in physical alginate gels: a rheological and dynamic light scattering investigation, Soft Matter 9 (2013) 10005, https://doi.org/10.1039/c3sm52006d.

[44] G. Skjåk-Bræk, H. Grasdalen, O. Smidsrød, Inhomogeneous polysaccharide ionic gels, Carbohydrate polymers 10 (1989) 31–54, https://doi.org/10.1016/0144-8617(89)90030-1.

[45] K. Ingar Draget, K. Østgaard, O. Smidsrød, Homogeneous alginate gels: A technical approach, Carbohydrate polymers 14 (1990) 159–178, https://doi.org/10.1016/0144-8617(90)90028-Q.

[46] C. Oelschlaeger, F. Bossler, N. Willenbacher, Synthesis, Structural and Micromechanical Properties of 3D Hyaluronic Acid-Based Cryogel Scaffolds, Biomacromolecules 17 (2016) 580–589, https://doi.org/10.1021/acs.biomac.5b01529.

[47] N. Golafshan, R. Rezahasani, M. Tarkesh Esfahani, M. Kharaziha, S.N. Khorasani, Nanohybrid hydrogels of laponite: PVA-Alginate as a potential wound healing material, Carbohydrate polymers 176 (2017) 392–401, https://doi.org/10.1016/j.carbpol.2017.08.070.

[48] M.S. Islam, M.R. Karim, Fabrication and characterization of poly(vinyl alcohol)/alginate blend nanofibers by electrospinning method, Colloids and Surfaces A: Physicochemical and Engineering Aspects 366 (2010) 135–140, https://doi.org/10.1016/j.colsurfa.2010.05.038.

[49] Q. Wei, R. Yang, D. Sun, J. Zhou, M. Li, Y. Zhang, Y. Wang, Design and evaluation of sodium alginate/polyvinyl alcohol blend hydrogel for 3D bioprinting cartilage scaffold: molecular dynamics simulation and experimental method, Journal of Materials Research and Technology 17 (2022) 66–78, https://doi.org/10.1016/j.jmrt.2021.12.130.

[50] C. Weis, C. Oelschlaeger, D. Dijkstra, M. Ranft, N. Willenbacher, Microstructure, local dynamics, and flow behavior of colloidal suspensions with weak attractive interactions, Scientific reports 6 (2016) 33498, https://doi.org/10.1038/srep33498.

[51] S. Alberti, A. Gladfelter, T. Mittag, Considerations and Challenges in Studying Liquid-Liquid Phase Separation and Biomolecular Condensates, Cell 176 (2019) 419–434, https://doi.org/10.1016/j.cell.2018.12.035.

[52] C. Fernández-Rico, T. Sai, A. Sicher, R.W. Style, E.R. Dufresne, Putting the Squeeze on Phase Separation, JACS Au 2 (2022) 66–73, https://doi.org/10.1021/jacsau.1c00443.

[53] S. Jabbari-Farouji, H. Tanaka, G.H. Wegdam, D. Bonn, Multiple nonergodic disordered states in Laponite suspensions: a phase diagram, Physical review, E, Statistical, nonlinear, and soft matter physics 78 (2008) 61405, https://doi.org/10.1103/PhysRevE.78.061405.

[54] M. Pilavtepe, S.M. Recktenwald, R. Schuhmann, K. Emmerich, N. Willenbacher, Macro- and microscale structure formation and aging in different arrested states of Laponite dispersions, Journal of Rheology 62 (2018) 593–605, https://doi.org/10.1122/1.5001382.

[55] L. Li, L. Harnau, S. Rosenfeldt, M. Ballauff, Effective interaction of charged platelets in aqueous solution: investigations of colloid laponite suspensions by static light scattering and small-angle x-ray scattering, Physical review, E, Statistical, nonlinear, and soft matter physics 72 (2005) 51504, https://doi.org/10.1103/PhysRevE.72.051504.
[56] T.B. Becher, C.B. Braga, D.L. Bertuzzi, M.D. Ramos, A. Hassan, F.N. Crespilho, C. Ornelas, The structure-property relationship in LAPONITE® materials: from Wigner glasses to strong self-healing hydrogels formed by non-covalent interactions, Soft Matter 15 (2019) 1278–1289, https://doi.org/10.1039/c8sm01965g.
[57] A. Sheikhi, S. Afewerki, R. Oklu, A.K. Gaharwar, A. Khademhosseini, Effect of ionic strength on shear-thinning nanoclay-polymer composite hydrogels, Biomaterials science 6 (2018) 2073–2083, https://doi.org/10.1039/C8BM00469B.
[58] F. Xie, C. Boyer, V. Gaborit, T. Rouillon, J. Guicheux, J.-F. Tassin, V. Geoffroy, G. Réthoré, P. Weiss, A Cellulose/Laponite Interpenetrated Polymer Network (IPN) Hydrogel: Controllable Double-Network Structure with High Modulus, Polymers 10 (2018), https://doi.org/10.3390/polym10060634.
[59] M. Ghadiri, W. Chrzanowski, W.H. Lee, A. Fathi, F. Dehghani, R. Rohanizadeh, Physico-chemical, mechanical and cytotoxicity characterizations of Laponite®/alginate nanocomposite, Applied Clay Science 85 (2013) 64–73, https://doi.org/10.1016/j.clay.2013.08.049.
[60] D.M. Knapp, V.H. Barocas, A.G. Moon, Rheology of reconstituted type I collagen gel in confined compression, Journal of Rheology 41 (1997) 971, https://doi.org/10.1122/1.550817.
[61] Z. Xing, H. Lu, Y.Q. Fu, Local conservation law of rubber elasticity in hydrogel networks undergoing microphase separation and toughening, Polymer 222 (2021), https://doi.org/10.1016/j.polymer.2021.123656 123656.